Ginzburg-Landau model for mode competition and single-mode operation of a free-electron laser

C. S. Ng and A. Bhattacharjee
Department of Physics and Astronomy, The University of Iowa, Iowa City, Iowa 52242
(Received 23 April 1998)

Mode competition of a free-electron laser is modeled by the Ginzburg-Landau equation. The stability of a single-mode solution is analyzed, and connections are established with known instabilities of the Ginzburg-Landau equation. It is found that the principal mode with the largest gain is always stable and hence there is no Benjamin-Feir instability. However, the Eckhaus (or phase) instability generally occurs if the frequency of a mode lies outside of a designated range centered on the principal mode. Under certain conditions, the Eckhaus instability can cause a sudden chaotization and spikiness in the radiation field. Analytical criteria and scaling for single-mode operation are given and tested by numerical simulations. A theoretical controversy on single-mode operation of the free-electron laser at the University of California at Santa Barbara is resolved. [S1063-651X(98)16009-9]

PACS number(s): 41.60.Cr, 52.35.Mw

I. INTRODUCTION

The complex Ginzburg-Landau equation (GLE) is a partial differential equation of the general form

$$\frac{\partial A}{\partial z}=A+(1+ic_1)\frac{\partial^2 A}{\partial t^2}-(1+ic_2)|A|^2A, \tag{1}$$

where $A(z,t)$ is a complex scalar field, z and t are real independent variables, and c_1 and c_2 are real parameters. The main purpose of this paper is to analyze the issue of mode competition and single-mode operation of a free-electron laser (FEL) using the GLE as a nonlinear model of the radiation field. In so doing, we establish connections with a rich mathematical literature (with antecedents in hydrodynamics [1–8]) on single-mode solutions of the GLE, their stability, and the chaotic dynamics following an instability. These connections allow us to view FEL operation in the nonlinear regime from a new perspective and resolve an old controversy.

The GLE was first proposed as a model for the nonlinear evolution of the radiation field $A(z,t)$ in a FEL by Cai and Bhattacharjee [9], who were motivated by observations of optical ''spiking'' in several experiments [10–13]. There are other theoretical models of FEL's, which also arrive at a reduced version of the GLE [14–16]. In these models, the radiation field is assumed to be a function only of z. Consequently, they arrive at an ordinary differential equation that can be obtained from Eq. (1) by simply setting the time derivative to zero. This reduced version of the GLE, derived in [16] under the assumption that the FEL radiation field is already in a single-mode state (''supermode''), can be used to describe the linear and nonlinear properties of the single mode. But unlike the partial differential equation (1), it cannot describe the interesting nonlinear dynamics of mode competition—how a stable single-mode solution can evolve out of an initial condition involving multiple modes, or how an unstable single-mode solution can lead to the spontaneous nonlinear excitation of multiple modes.

The possibility that a FEL can produce a powerful and coherent optical beam of a single frequency is potentially of great interest for many applications. There is experimental evidence from the FEL at the University of California at Santa Barbara (UCSB) that such a possibility is realizable with long-pulse electron beams [17]. Although there is theoretical controversy [18,19] as to whether the FEL at UCSB actually attained a single-mode state, there is little doubt that the optical beam in the experiment showed a clear tendency to operate on a very narrow bandwidth.

We show by analysis and numerical simulation that the GLE provides useful insight on how single-mode operation evolves out of the nonlinear interaction of multiple modes. In particular, it yields specific analytical conditions on when single-mode operation is stable, when instability occurs, and describes the impulsive nonlinear growth of the instability leading to a chaotic and spiky optical beam. We show that the model helps resolve the theoretical controversy as to whether single-mode operation was realized in the UCSB FEL [17]. We also discuss briefly the implications of the model for self-amplified spontaneous emission in the x-ray FEL device proposed to operate at the Stanford Linear Accelerator Center (SLAC).

II. DERIVATION OF THE GLE

We begin with a new derivation of the GLE for a FEL amplifier in the high-gain regime. We do not consider the problem of sideband instabilities [20], which introduce additional complications well beyond the scope of the present paper. We start with the standard one-dimensional equations for a Compton FEL:

$$\frac{d\gamma_j}{dz}=-\frac{k_s a_s a_w}{\gamma_j}\sin(\psi_j+\phi), \tag{2a}$$

$$\frac{d\psi_j}{dz}=k_w\left[1-\frac{\gamma_r^2}{\gamma_j^2}\right]+\frac{k_s a_w a_s}{\gamma_j^2}\cos(\psi_j+\phi), \tag{2b}$$

$$\frac{du}{dz}=i\frac{a_w\omega_p^2}{2k_s c^2}\left\langle\frac{\exp(-i\psi)}{\gamma}\right\rangle. \tag{2c}$$

Here z is along the axis of the undulator that has magnetic vector potential $\mathbf{A}_w$ and wave number k_w; $\psi_j+\phi$ is the phase of the jth electron (of rest mass m, charge e, and energy $\gamma_j mc^2$) with respect to the radiation field determined by the vector potential $\mathbf{A}_s$, reference frequency ω_s, and wave number $k_s=\omega_s/c$; $a_w\equiv eA_w/mc^2$, $a_s\equiv eA_s/mc^2$, $u\equiv a_s\exp(i\phi)$; $\gamma_j^2\equiv k_s(1+a_w^2)/2k_w$ is the resonant energy and ω_p is the plasma frequency. It has been shown [21] that Eqs. (2a)–(2c) are approximated well by the reduced set of equations

$$\frac{dA}{dz}=i\delta A+igx, \tag{3a}$$

$$\frac{dx}{dz}=-ihy, \tag{3b}$$

$$\frac{dy}{dz}=ifA-2i[hy_0(y-xy_0)-\delta xy_0+f(x^*A+A^*x)x], \tag{3c}$$

for collective variables $x\equiv\langle\exp[-i(\psi_j-\psi_r)]\rangle$, $y\equiv\langle[(\gamma_j-\gamma_0)/\gamma_0]\exp[-i(\psi_j-\psi_r)]\rangle$, and $A\equiv u\exp(i\psi_r)$, where $d\psi_r/dz\equiv\delta\equiv k_w(1-\gamma_r^2/\gamma_0^2)$ and γ_0 is the initial energy of the electron beam; $f\equiv k_s a_w/2\gamma_0^2$, $g\equiv\omega_p^2 a_w/2k_s\gamma_0 c^2$, $h\equiv k_s(1+a_w^2)/\gamma_0^2$. Equations (3a)–(3c) admit the energy conservation relation $y_0\equiv\langle(\gamma_j-\gamma_0)/\gamma_0\rangle=f[|A(z=0)|^2-|A|^2]/g\approx -f|A|^2/g$. We linearize and factorize Eqs. (3a)–(3c) to obtain

$$\left(\frac{d}{dz}-i\lambda_1\right)\left(\frac{d}{dz}-i\lambda_2\right)\left(\frac{d}{dz}-i\lambda_3\right)A=0, \tag{4}$$

where $\lambda_1,\lambda_2,\lambda_3$ are the three roots of the equation $\lambda_0^3-\delta\lambda_0^2+fgh=0$. At resonance ($\delta=0$) we obtain $fgh=8\rho^3k_w^3$, where $\rho=\gamma_0^{-1}(a_w\omega_p/4ck_w)^{2/3}$ is the so-called Pierce parameter. The linear solution is quickly dominated by the most unstable eigenvalue, and can be written (approximately) as $A\propto\exp(i\lambda_0 z)$, where $\lambda_0(=\lambda_r+i\lambda_i)$ is the eigenvalue with a negative imaginary part. In Fig. 1, the solid curve shows a typical linear gain $(-\lambda_i)$ as a function of ω for a small value of ρ, where ω is measured in units of $2\gamma_0^2ck_w/(1+a_w^2)$. In this unit, $\omega=1$ is the frequency when the resonance condition $\delta=0$ is satisfied. For small values of ρ, the resonant ω is close to the frequency ω_m at which the gain is maximum.

Including the effect of the first-order nonlinearity in $|A|^2$, Eq. (4) becomes

$$\prod_{j=1,3}\left(\frac{d}{dz}-i\lambda_j-i\beta|A|^2\right)A\approx 0, \tag{5}$$

where $d|A|^2/dz\approx -2\,\mathrm{Im}\,\lambda_0|A|^2$ and

$$\beta=\frac{-2fh(\lambda_0-\delta)(\lambda_0+2\,\mathrm{Re}\,\lambda_0-\delta)/g}{2\,\mathrm{Im}\,\lambda_0[2\,\mathrm{Im}\,\lambda_0-i(3\lambda_0-\delta)]-3\lambda_0^2+2\delta\lambda_0}. \tag{6}$$

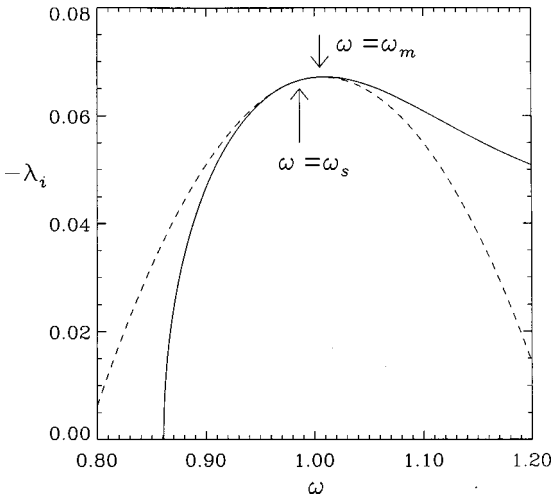

FIG. 1. Solid line: the linear gain $(-\lambda_i)$ as a function of the frequency ω for $\rho\approx 3.87\times10^{-2}$, with λ_i measured in units of k_w and ω measured in units of $2\gamma_0^2ck_w/(1+a_w^2)$. Dashed line: the linear gain curve for the GLE, expanded around the reference frequency $\omega=\omega_s$. The solid gain curve has a maximum at $\omega=\omega_m$, which is close to the frequency of maximum gain of the dashed curve.

We now write $d/dz\rightarrow\partial/\partial z+c^{-1}\partial/\partial t$, and treat A as a function of z and t with a Fourier spectrum in time. We expand $\lambda_0(\omega)$ around a reference frequency $\omega=\omega_s$,

$$\lambda_0(\omega)\approx\lambda_0(\omega_s)+\frac{\partial\lambda_0}{\partial\omega}\Delta\omega+\frac{1}{2}\frac{\partial^2\lambda_0}{\partial\omega^2}(\Delta\omega)^2$$

$$\rightarrow\lambda_0(\omega_s)+\frac{\partial\lambda_0}{\partial\omega}\,i\,\frac{\partial}{\partial t}-\frac{1}{2}\frac{\partial^2\lambda_0}{\partial\omega^2}\frac{\partial^2}{\partial t^2}, \tag{7}$$

where $\Delta\omega=\omega-\omega_s$. It follows from Eqs. (5) and (7) that

$$\frac{\partial A}{\partial z}=i\lambda_0A-\frac{1}{\nu_g}\frac{\partial A}{\partial t}-\frac{i\alpha}{2}\frac{\partial^2A}{\partial t^2}+i\beta|A|^2A, \tag{8}$$

where $\nu_g\equiv c/(1+c\partial\lambda_0/\partial\omega)$ and $\alpha\equiv\partial^2\lambda_0/\partial\omega^2$ are complex parameters. We now write $1/\nu_g=\mu_r+i\mu_i$, $\alpha=\alpha_r+i\alpha_i$, $\beta=\beta_r+i\beta_i$, and apply the transformations $A=A_0A'\exp[i(Kz'+\Omega t')]$, $z=z_0z'$, $t=t_0t'-z/\nu_0$, where

$$z_0=1/(-\lambda_i+\mu_i^2/2\alpha_i),\quad t_0^2=\alpha_iz_0/2,$$

$$\Omega=\mu_it_0/\alpha_i,\quad 1/\nu_0=-\mu_r+\alpha_r\mu_i/\alpha_i, \tag{9}$$

$$K=(\lambda_r-\alpha_r\mu_i^2/2\alpha_i^2)z_0,\quad A_0^2=1/z_0\beta_i.$$

Equation (8) then becomes the GLE in standard form (1), where $c_1=-\alpha_r/\alpha_i$ and $c_2=-\beta_r/\beta_i$ are real parameters and all primes have been dropped for notational convenience.

In Eq. (7), truncation of the Taylor series at second order implies that we approximate the linear gain curve around $\omega=\omega_s$ by a parabola. In Fig. 1, this parabola is shown as the dashed curve with the reference frequency ω_s chosen to be slightly less than the maximum gain frequency ω_m. For the

GLE, the maximum of the gain parabola is obtained at the frequency $\omega_s-\mu_i/\alpha_i$, which is a good approximation for the maximum gain frequency ω_m of the true gain curve with $\omega_m=\omega_s-\mu_i/\alpha_i+O(|\omega_m-\omega_s|^2)$ provided ω_s is close to ω_m. Thus the frequencies for maximum gain of the two curves in Fig. 1 are very close to each other, as shown.

III. SINGLE-MODE SOLUTION AND ITS INSTABILITIES

Equation (1) has an exact single-mode solution of the form

$$A=\sqrt{1-\omega_0^2}\ \exp\ i\{[-c_2+(c_2-c_1)\omega_0^2]z-\omega_0 t+\phi_0\}, \tag{10}$$

where ω_0,ϕ_0 are real constants. By Eqs. (7) and (9), the frequency of the radiation field is given by $\omega=\omega_s-\mu_i/\alpha_i+\omega_0/t_0$.

Single-mode solutions of the GLE may suffer two types of instabilities [1–5]. The first type is known as the Benjamin-Feir instability when every mode is unstable. If such an instability were operative in a FEL, it would be impossible to realize single-mode operation. The second type is known as the Eckhaus instability, which is said to occur when a single-mode solution is stable if its frequency lies within a designated range, but unstable outside of that range. We now analyze these instabilities in the context of FEL's.

We first consider the maximum gain mode with $\omega_0=0$. (We show below that if the mode with maximum gain is unstable, so are all other modes.) The linear stability of this mode can be examined by writing the perturbed radiation field as $A=(1+a)\exp i(-c_2z+\phi_0+\theta)$, where $a=\tilde{a}\cos(\omega_d t)$ and $\theta=\tilde{\theta}\cos(\omega_d t)$ are small and real perturbations [5]. Linearizing Eq. (1), we obtain

$$\frac{d}{dz}\begin{pmatrix}\tilde{a}\\ \tilde{\theta}\end{pmatrix}=\begin{pmatrix}-2-\omega_d^2 & c_1\omega_d^2\\ -2c_2-c_1\omega_d^2 & -\omega_d^2\end{pmatrix}\begin{pmatrix}\tilde{a}\\ \tilde{\theta}\end{pmatrix}. \tag{11}$$

The eigenvalues for exponential solutions of Eq. (11) are

$$\Lambda=-(1+\omega_d^2)\pm\sqrt{(1+\omega_d^2)^2-(1+c_1^2)\omega_d^4-2(1+c_1c_2)\omega_d^2}. \tag{12}$$

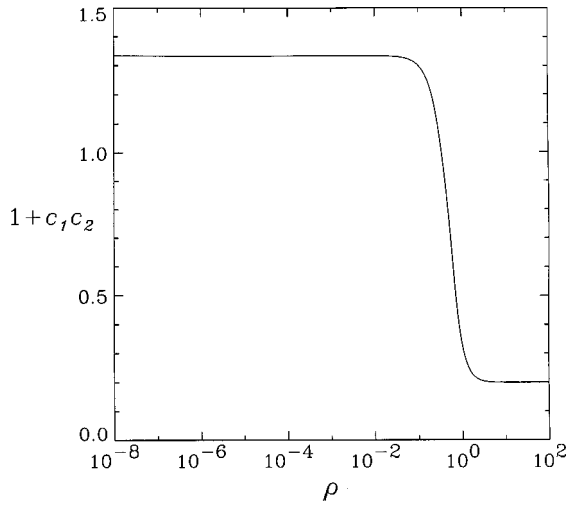

FIG. 2. The Benjamin-Feir stability parameter $1+c_1c_2$, evaluated at maximum gain with $\omega_s=\omega_m$ and $\omega_0=0$, as a function of the Pierce parameter ρ.

In order for the mode to be unstable, Λ must have a positive real part (for some ω_d), which is possible only if $1+c_1c_2<0$. For the FEL, if we choose the reference frequency as the frequency with maximum gain ($\omega_s=\omega_m$), it is easy to see that the quantity $1+c_1c_2$ depends only on ρ. In the limit $\rho\to0$, we obtain $\omega_m\to2\gamma_0^2ck_w/(1+a_w^2)$ and $1+c_1c_2\to4/3$, which implies that the mode is stable (in this limit). For nonzero values of ρ, since we do not have a simple analytical formula for either the parameter ω_m or the coefficient $1+c_1c_2$, we carry out a numerical calculation. In Fig. 2, we plot $1+c_1c_2$ as a function of ρ. Since most FEL's are characterized by small values of ρ, we see that $1+c_1c_2$ is positive in the regime of physical interest. We conclude that the single mode $\omega=\omega_m$ with maximum gain is stable, and hence there is no Benjamin-Feir instability. This is consistent with the earlier findings of [18] and [19].

Although the maximum gain mode with $\omega_0=0$ is linearly stable, a mode with $|\omega_0|\neq0$ may be unstable to the Eckhaus instability. To examine this possibility, we consider the linearized equations

$$\frac{d}{dz}\begin{pmatrix}\tilde{a}\\ \tilde{\theta}\end{pmatrix}=\begin{pmatrix}-2a_0-\omega_d^2-2ic_1\omega_0\omega_d & c_1a_0\omega_d^2-2ia_0\omega_0\omega_d\\ -2c_2a_0-(c_1\omega_d^2-2i\omega_0\omega_d)/a_0 & -\omega_d^2-2ic_1\omega_0\omega_d\end{pmatrix}\begin{pmatrix}\tilde{a}\\ \tilde{\theta}\end{pmatrix}, \tag{13}$$

where $a_0^2\equiv1-\omega_0^2>0$. The corresponding eigenvalues are

$$\Lambda=\omega_0^2-1-\omega_d^2-2ic_1\omega_0\omega_d\pm\{(\omega_0^2-1)^2-2c_1\omega_d^2[c_2(1-\omega_0^2)+c_1\omega_d^2/2]+4\omega_0^2\omega_d^2+4ic_2\omega_0\omega_d(1-\omega_0^2)+4ic_1\omega_0\omega_d^3\}^{1/2}. \tag{14}$$

In the limit of small ω_d, Eq. (14) reduces to

$$\Lambda\xrightarrow{\omega_d\to0}\begin{cases}-2(1-\omega_0^2),\\ -2\left[1+c_1c_2+\dfrac{2\omega_0^2}{\omega_0^2-1}(1+c_2^2)\right]\dfrac{\omega_d^2}{2}+2i\omega_0\omega_d(c_2-c_1).\end{cases} \tag{15}$$

We observe that the single mode of frequency ω_0 is unstable if the square bracket of the lower expression in Eq. (15) is negative. Note that this is true for every ω_0 if $1+c_1c_2<0$; however, if $1+c_1c_2>0$, the mode will be unstable when $\omega_0^2>(1+c_1c_2)/(3+c_1c_2+2c_2^2)$, which can always be satisfied in the range $1-\omega_0^2>0$. Therefore, the Eckhaus instability will always occur.

From Eq. (13), in the small-ω_d limit, we see that the unstable eigenvector is phase-aligned. In fact, the ratio of the phase component to the amplitude component in an eigenvector is given by

$$\frac{\tilde{\theta}}{\tilde{a}}=\frac{2a_0^2+\omega_d^2+2ic_1\omega_0\omega_d+\Lambda}{c_1a_0\omega_d^2-2ia_0\omega_0\omega_d}, \tag{16}$$

which is finite in the limit of zero ω_d for the upper eigenvalue in Eq. (15), but tends to infinity for the lower unstable eigenvalue. In this limit, the Eckhaus instability is the phase instability discussed in [19]. Furthermore, we see from Eqs. (15) and (16) that for a stable mode, the decay rate of the amplitude perturbation (for small ω_d) is much larger than that of the phase perturbation, as emphasized in [19].

We define the spectral width as $\Delta\omega_d\equiv\langle(\omega_d-\langle\omega_d\rangle)^2\rangle^{1/2}$, where $\langle\omega_d\rangle\equiv\int_{-\infty}^{\infty}\omega_d\tilde{\theta}(\omega_d,z)d\omega_d/\int_{-\infty}^{\infty}\tilde{\theta}(\omega_d,z)d\omega_d$. From Eq. (15), we obtain $\tilde{\theta}(\omega_d,z)=\tilde{\theta}(\omega_d,0)\exp(\Lambda z)\sim\tilde{\theta}_0\exp[(-h_1\omega_d^2+ih_2\omega_d)z]$ for the lower eigenvalue, where $\tilde{\theta}_0$, h_1, and h_2 are constants. Thus, we deduce that the spectral half-width decays as $\Delta\omega_d=(2h_1z)^{-1/2}\propto z^{-1/2}$, consistent with the scaling reported in [19]. Note that this scaling applies to a continuum of modes. As shown below, for discrete modes the scaling holds until the spectral width is reduced to about one mode, after which the width decays much faster than $z^{-1/2}$.

IV. NUMERICAL SIMULATIONS

To test the analytical predictions discussed above, we have developed a pseudospectral computer code that integrates the GLE. The coefficients c_1 and c_2 are calculated for the parameters of the UCSB FEL [17]: $k_w=175\ \mathrm{m}^{-1}$, $k_s=15.7\ \mathrm{mm}^{-1}$, $a_w=0.3$, $\omega_p/ck_w=0.012$, and $\gamma_0=7$. (With these parameters, $\rho\approx2.87\times10^{-2}$ and the effective current density is $4.4\times10^4\ \mathrm{A\ m}^{-2}$.)

We first consider the maximum gain mode $\omega_s=\omega_m\approx750$ GHz, which is stable because $c_1\approx-0.580$, $c_2\approx-0.574$ and the stability condition $1+c_1c_2>0$ is satisfied. We use periodic boundary conditions in t and expand A in a Fourier series of terms with relative frequencies that are multiples of the frequency width $\delta\omega_s$. The simulation is initialized (at $z=0$) with random small values distributed over 2048 Fourier modes. The unit of time is chosen such that the ratio of longitudinal frequency spacing to the principal frequency is given by $\delta\omega_s/\omega_s=2\times10^{-3}/75$, similar to that in the UCSB experiment [17].

The solid curve in Fig. 3 shows the evolution of the (normalized) spectral width $\Delta\omega$ (in units of the number of longitudinal modes) as a function of z/c (in units of 1 μs). [Here z is the actual physical distance along the axis, not the dimensionless variable in Eq. (1).] We see that $\Delta\omega$ decays by about two decades when z increases by roughly four decades—consistent with the analytical scaling $\Delta\omega\propto z^{-1/2}$, which appears to persist until $\Delta\omega$ is reduced to about one mode. The dotted curve is the (normalized) spectral width $\Delta\omega_A$, calculated on the basis of the frequency spectrum of the amplitude of A. We note that $\Delta\omega$ and $\Delta\omega_A$ are of the same order of magnitude for a short, initial interval in z. Thereafter, $\Delta\omega_A$ decays at a much faster rate ($\propto z^{-1}$) than $\Delta\omega$. This suggests that the amplitude of A becomes approximately constant well before the full solution (including the phase) attains a true single-mode state. The phase perturbations decay much slower than amplitude perturbations, in agreement with [19]. The amplitude becomes roughly constant (when $\Delta\omega_A\sim1$) at $z/c\sim5$ μs. At this stage, $\Delta\omega$ can be viewed as a ''macromode,'' consisting of 10–20 eigenmodes. This macromode eventually decays to one eigenmode at $z/c\sim1$ ms, but that is much longer than the electron pulse length (~50 μs) in the experiment.

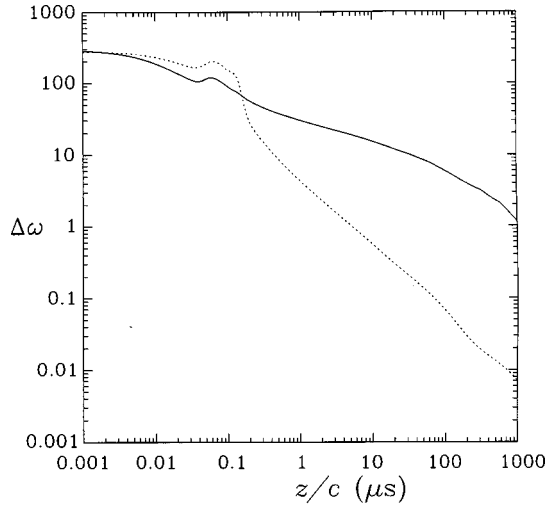

FIG. 3. The evolution along z/c (μs) of $\Delta\omega$ (solid line) and $\Delta\omega_A$ (dotted line) (in units of the number of longitudinal modes) in a simulation of the GLE initialized with small random Fourier amplitudes for $c_1\approx-0.580$ and $c_2\approx-0.574$. The final state is a single-mode solution with frequency close to the central frequency ω_m.

The spectral measurements of the UCSB FEL, reported in [22], appear to be consistent with our interpretation. We illustrate this further in Fig. 4, which provides detailed information on the radiation field at $z/c\approx2.1$ μs. Figure 4(a) of the Fourier amplitude spectrum shows nearly 50 modes in the frequency half-width. It is, therefore, not surprising that the time series of the real part of the amplitude, A_r, has a very spiky structure [Fig. 4(b)] and the phase ϕ exhibits large temporal variations [Fig. 4(c)]. However, this temporal structure is not seen in $|A|^2$ [Fig. 4(d)], which has already relaxed to a nearly constant value.

It is interesting to note that our scaling results are derived from equations that apply to a high-gain FEL amplifier, as in [18], but are actually in agreement with the ''klystron model'' developed in [19] for a FEL oscillator. We do not believe this is mere coincidence. It suggests that the nonlin-

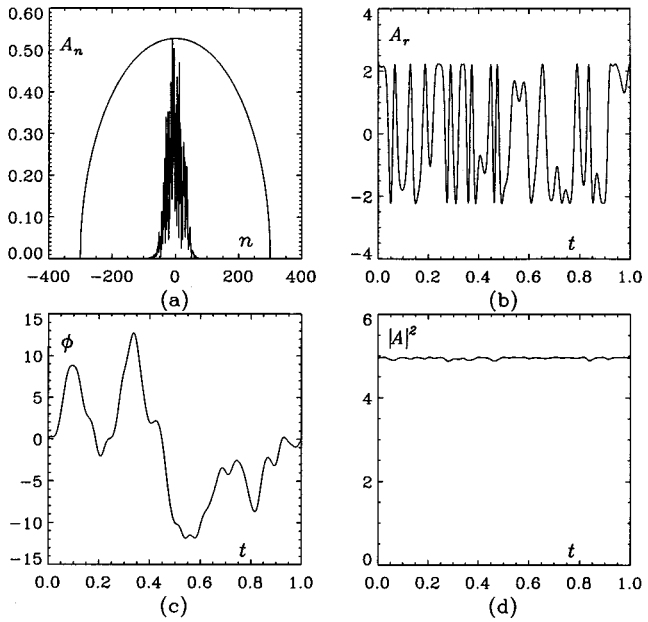

FIG. 4. (a) Fourier amplitude A_n as a function of the Fourier mode number n with the gain parabola plotted in arbitrary units, (b) A_r, the real part of the amplitude, (c) the phase ϕ, and (d) the amplitude square $|A|^2$ of the radiation field plotted as a function of time in one simulation period, which is about 31.4 μs at $z/c \approx 2.1$ μs in the run with the parameters of Fig. 3.

ear physics of mode competition (in the absence of sidebands) is probably similar in an amplifier and an oscillator. A derivation of the GLE from the low-gain oscillator equations (including the appropriate boundary conditions) will be the subject of a future paper.

Next, for the same FEL parameters but with 512 Fourier modes, we consider a single-mode solution with $\omega_s = 0.977\omega_m$ and $\omega_0 = \mu_i t_0/\alpha_i$, which corresponds to $c_1 \approx -0.009\,44$ and $c_2 \approx -4.25$. When we add a small perturbation, the system becomes unstable to the Eckhaus instability although the principal mode is stable. Two distinct types of behavior can then occur: either the system undergoes spontaneous self-adjustment by shifting the unstable mode to another mode inside the stable range, or the instability grows virulently, exciting multiple modes and producing a chaotic state. The type of behavior seen in any particular case depends extremely sensitively on the initial conditions. In Figs. 5–7, we illustrate by example the second type of behavior. The upper (lower) curve in Fig. 5 shows $\Delta\omega$ ($\Delta\omega_A$) as a function of z. Both quantities—$\Delta\omega$ as well as $\Delta\omega_A$—are of the same order of magnitude initially due to the smallness of the perturbation initiating the instability. This is followed by a range in z over which $\Delta\omega$ is larger than $\Delta\omega_A$ by more than an order of magnitude, although neither quantity is very large. Thus, in the linear regime, the amplitude perturbation grows more slowly than the phase perturbation, consistent with our interpretation of the Eckhaus instability as a phase instability. In the nonlinear regime, due to strong mode coupling, both $\Delta\omega$ and $\Delta\omega_A$ grow very rapidly and impulsively, and the system evolves to a nonlinear state consisting of approximately 40 modes. Although the principal mode (as well as modes in a narrow range around the principal mode) is linearly stable because $1 + c_1 c_2 > 0$, the system does not decay to a single-mode state. Instead, it evolves to a chaotic

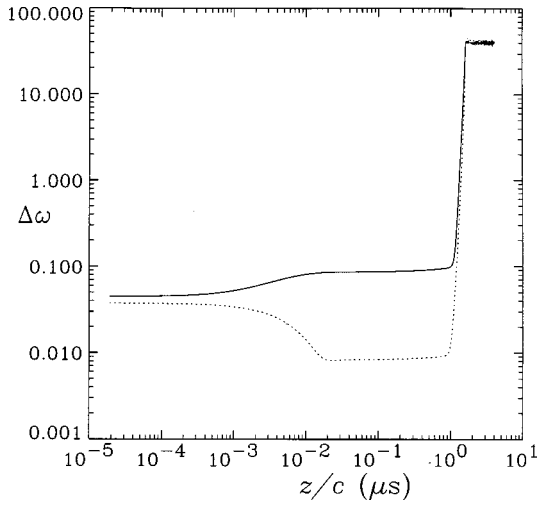

FIG. 5. The evolution along z/c (μs) of $\Delta\omega$ (solid curve) and $\Delta\omega_A$ (dotted curve) for the case of $c_1 \approx -0.009\,44$ and $c_2 \approx -4.25$ starting with an Eckhaus-unstable single-mode solution.

state, at least as long as we are able to follow it numerically, leading to ''phase turbulence'' of the type reported in [4]. Figure 6 shows the magnitude A_n of the Fourier modes, indexed by n, of one such chaotic state, with the parabola showing the shape of the gain curve. (The precise value of z is not important here since we will see the same qualitative picture for any z within the chaotic state.) We see that the energy is distributed over a wide range within the positive gain region, although the distribution is not as even between the competing modes as the gain curve might suggest. As is evident from Fig. 7, the power in this chaotic state is very spiky. The width of the spikes varies over a rather large range, with some spikes characterized by widths of the order of $(-\alpha_i/2\lambda_i)^{1/2}$, given by the solitary-wave solution of the GLE [9]. [The width of the solitary-wave solution is represented in Fig. 7 as the width of the box (thick line) in the middle top region.] It thus remains a possibility that some of the spikes observed in experiments [10–13] are a result of the Eckhaus instability of a single mode even without the

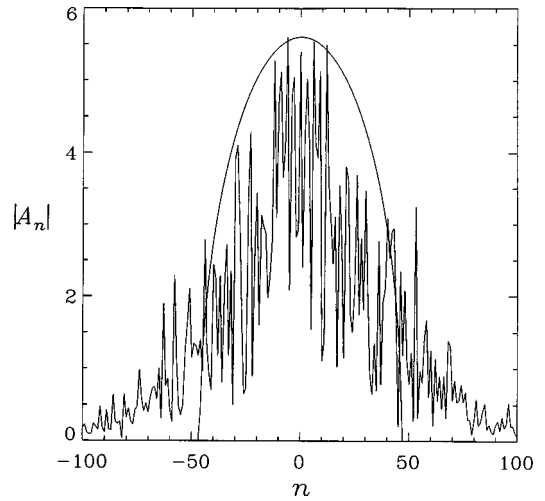

FIG. 6. Amplitude A_n in unit of 10^{-5} m c^2/e, as a function of the Fourier mode number n for the same parameters as Fig. 5. The gain curve, a parabola, is also plotted in arbitrary units.

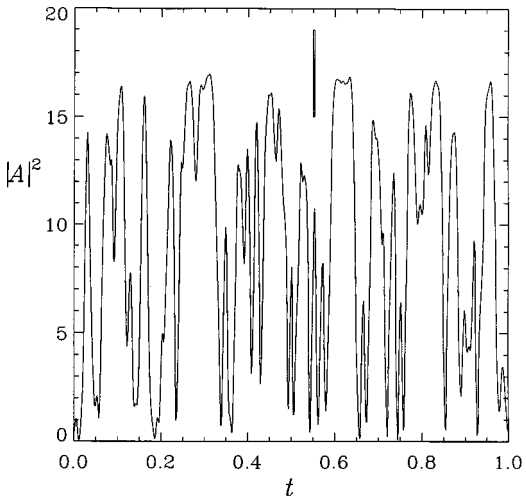

FIG. 7. Amplitude square $|A|^2$, in unit of 10^{-10} m^2 c$^4/e^2$, as a function of time in one simulation period which is about 12.7 μs at the same z as Fig. 6. The width of the box (thick line, middle top) represents the solitary wave width $(-\alpha_i/2\lambda_i)^{1/2}$.

intervention of sideband instabilities.

We now apply the GLE to mode narrowing in the proposed Linac Coherent Light Source (LCLS) device at SLAC, which is expected to generate x rays from noise [23]. At the end of a single pass of the undulator, the radiation field is in the early nonlinear saturation phase (as seen in [23]), and sideband amplitudes are sufficiently small that the GLE remains applicable. Figure 8 shows the results of a simulation of the GLE using LCLS parameters [23], with random initial condition of the radiation field. While Fig. 8(a) shows the time-averaged radiation power along the undulator axis, Fig. 8(b) shows the evolution of $\Delta\omega$ and $\Delta\omega_A$. We see that the spectral width decreases initially in the linear phase, then increases slightly when the power starts to saturate, and then decreases again. With an undulator 100 m long, the planned LCLS device exhibits some tendency for mode narrowing, but since $\Delta\omega_A$ is of the same order as $\Delta\omega$, we cannot expect either the multimode amplitude or the phase perturbations to decay in a single pass. For a longer undulator, the GLE must be modified to include the effects of sidebands, which may broaden the spectrum. This is left to future work.

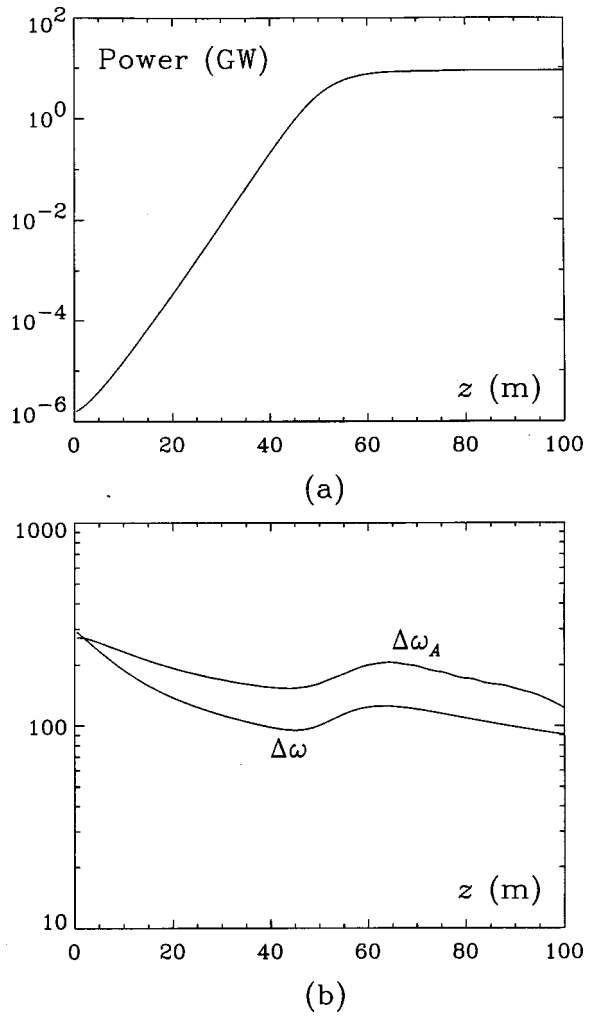

FIG. 8. (a) Time-averaged radiation field power (*GW*) as a function of undulator length z (m) in a simulation of the GLE using LCLS parameters with random initial condition. (b) The evolution of $\Delta\omega$ and $\Delta\omega_A$ (in unit of the number of modes) in simulation (a).

V. SUMMARY

The GLE gives a remarkably precise and detailed description of mode competition and single-mode operation of a FEL. We have obtained analytical conditions for the Benjamin-Feir and Eckhaus instabilities of a single-mode solution. We have shown that the mode with maximum gain is always stable, and hence there is no Benjamin-Feir instability. However, the Eckhaus (or phase instability) always occurs. We have verified the analytical results by simulations, and examined conditions under which stable single-mode operation can occur, with specific applications to the UCSB FEL. On the basis of our results, we conclude that single-mode operation did not occur in the UCSB FEL experiment [17].

When the Eckhaus instability occurs, it can lead to two distinct types of behavior: either the system undergoes spontaneous self-adjustment by shifting the unstable mode to another mode inside the stable range, or the instability grows virulently, exciting multiple modes and producing a chaotic state. The second type of behavior can thwart single-mode operation, and in the nonlinear regime, produce a sudden and rapid chaotization of the optical signal. This is a regime that has not received sufficient attention in FEL experiments, which can be an interesting test-bed for theories of ''phase turbulence.''

ACKNOWLEDGMENTS

This research is supported by the U.S. Air Force Office of Scientific Research under Grant No. F49620-96-1-0068, and the U.S. Department of Energy under Grant No. DE-FG02-91ER40669.

[1] J. T. Stuart and R. C. DiPrima, Proc. R. Soc. London, Ser. A **362**, 27 (1978).
[2] C. S. Bretherton and E. A. Spiegel, Phys. Lett. **96A**, 152 (1983).
[3] P. Coullet, L. Gil, and J. Lega, Phys. Rev. Lett. **62**, 1619 (1989).
[4] B. I. Shraiman, A. Pumir, W. van Saarloos, P. C. Hohenberg, H. Chaté, and M. Holen, Physica D **57**, 241 (1992).
[5] T. Leweke and M. Provansal, J. Fluid Mech. **288**, 265 (1995).
[6] M. C. Cross and P. C. Hohenberg, Rev. Mod. Phys. **65**, 851 (1993).
[7] F. Cariello and M. Tabor, Physica D **39**, 77 (1985).
[8] N. Bekki and I. Nozaki, Phys. Lett. **110A**, 133 (1985).
[9] S. Y. Cai and A. Bhattacharjee, Phys. Rev. A **43**, 6934 (1991).
[10] R. W. Warren, J. C. Goldstein, and B. E. Newnam, Nucl. Instrum. Methods Phys. Res. A **250**, 104 (1986).
[11] J. W. Dodd and T. C. Marshall, IEEE Trans. Plasma Sci. **18**, 447 (1990).
[12] B. A. Richman, J. M. J. Madey, and E. Szarmes, Phys. Rev. Lett. **63**, 1682 (1989).
[13] L.-Y. Lin and T. C. Marshall, Phys. Rev. Lett. **70**, 2403 (1993).
[14] W. B. Colson and S. K. Ride, in *Physics of Quantum Electronics* (Addison-Wesley, Reading, MA, 1980), Vol. 7, p. 377.
[15] R. Bonifacio, C. Maroli, and A. Dragan, Opt. Commun. **76**, 353 (1990).
[16] N. Piovella, P. Chaix, G. Shvets, and D. A. Jaroszynski, Phys. Rev. E **52**, 5470 (1995).
[17] L. R. Elias, G. Ramian, J. Hu, and A. Amir, Phys. Rev. Lett. **57**, 424 (1986); L. R. Elias and I. Kimel, Nucl. Instrum. Methods Phys. Res. A **296**, 144 (1990).
[18] I. Kimel and L. R. Elias, Phys. Rev. A **38**, 2889 (1988); Nucl. Instrum. Methods Phys. Res. A **296**, 528 (1990); **341**, 191 (1994).
[19] B. Levush and T. M. Antonsen, Jr., Nucl. Instrum. Methods Phys. Res. A **272**, 375 (1988); **285**, 136 (1989); T. M. Antonsen, Jr. and B. Levush, Phys. Rev. Lett. **62**, 1488 (1989); Phys. Fluids B **1**, 1097 (1989).
[20] N. M. Kroll and M. N. Rosenbluth, in *Physics of Quantum Electronics* (Addison-Wesley, Reading, MA, 1980), Vol. 7, p. 147.
[21] R. Bonifacio, F. Casagrande, and L. De Salvo Souza, Phys. Rev. A **33**, 2836 (1986).
[22] B. G. Danly, S. G. Evangelides, T. S. Chu, R. J. Temkin, G. Ramian, and J. Hu, Phys. Rev. Lett. **65**, 2251 (1990).
[23] M. Cornacchia, SLAC-PUB-7433, March (1997).